Int. J. Electrochem. Sci., 15 **(2020)** 1005 – 1021, doi: 10.20964/2020.01.67

International Journal of
ELECTROCHEMICAL
SCIENCE
www.electrochemsci.org

Review

A Review on the Behavior of 308L Cladding Material and Their Corrosion in Nuclear Power Plants

Hassan Tukur[*], *Lu Yonghao*[*]

National Center for Material Service Safety, University of Science and Technology, Beijing, China P.R.
[*]E-mail: tingilin@yahoo.com, lu_yonghao@mater.ustb.edu.cn

Received: 17 June 2019 / *Accepted:* 20 November 2019 / *Published:* 30 November 2019

The shell materials in the main plants (pressure vessels, voltage regulators and steam generators) for nuclear equipment sometimes adopt surfacing welding on low alloy steel forging 308L austenitic stainless-steel welding layer manufacturing. Therefore, austenitic stainless-steel welding layer has an important influence in the nuclear power demanding service environment under the shell materials' performance for safe and effective operation. At the same time, effects of thermal aging cause a decline in performance of the stainless-steel surfacing layer, due to long service life of nuclear power plants. This is a key factor in the service safety of nuclear power plants. Several studies have been conducted on this phenomenon. In this paper, a review of the different studies on the microstructure, thermal aging behavior and its effect on oxidation behavior of domestic 308L stainless-steel surfacing layer is presented. Articles on small punching test and in-situ tensile test for deformation fracture behavior characteristics in phases of the microstructure of surfacing layer before and after thermal aging were reviewed. Also, researches on experiments combined with X-ray diffraction and X-ray photoelectron spectroscopy for detection of corrosion weight gain or loss, and oxidation film formed by the surfacing layer under high temperature and pressure, were presented. Through the review of experimental results in several articles, the laws and mechanisms of the changes in the microstructure, mechanical damage and high temperature water oxidation behavior of domestic surfacing materials 308L were clarified. The correlation between the property damage and microstructure evolution was revealed. Research gaps were brought out and conclusions as well as recommendations for further research were given.

Keywords: 308L stainless steel, weld surfacing, thermal aging, microstructure, mechanical property, oxidation behavior

1. INTRODUCTION

Cladding is defined as the application of a material with certain properties to the surface of the parent material that needs to be protected by means of heat source. Compared with other welding

technologies, the surfacing technology has the following advantages:(1) there is a good metallurgical combination between the cladding layer and the base material, and the spilling tendency of the clad layer is small;(2) the clad alloy can be selected or designed according to the needs, with great flexibility in the process [1, 2].Therefore, cladding technology is widely used in the preparation of nuclear power equipment.

Pressurized water reactor nuclear power plant is mainly divided into three circuits, including pressure vessel once upon components, voltage regulator, and the steam generator for nuclear power plants. The long-term safety and reliability of the primary circuit conditions must be guaranteed, so for the three-parts shell composition and performance of welding material and welding process has a certain requirement [3].

For these three parts of shell, the A508 low alloy steel with better comprehensive properties is widely used. But out of need to reduce the material corrosion, adopting overlaying welding technology in low alloy steel welding on the surface of three layers stainless steel, the first layer is transition layer near the parent metal, the main purpose is to break low alloy steel and stainless steel hard surfacing between the elements of the dilution, guarantee the performance of the cladding layer and the stainless steel surface layer. The stainless-steel weld bead layer is mainly to reduce corrosion. Currently, the widely used material is 309L/308L stainless steel, of which 309L stainless steel is transition layer and 308L stainless-steel is anti-corrosion layer [3].

2. METHODOLOGY

We systematically reviewed papers from 2004 to date and examine the literatures on issues relating to use of stainless-steel in nuclear plants. Data collected from Science Direct, Web of Science, Google Scholar, Scopus and Research Gate were utilized. Databases were broadly searched focusing on different topics and sub-topics namely; parameters of stainless-steel surfacing welding, composition and structure of stainless-steel surfacing layer, oxidation behavior of stainless-steel surfacing layer, composition and structure with high warm water oxide film, formation mechanism of water oxidation film at high temperature, stainless-steel tissue after thermal aging, mechanical properties after thermal aging, deformation behavior after thermal aging, corrosion behavior after thermal aging and summary of thermal aging behavior of stainless-steel. In this approach, the keywords were narrowed down on the influence of stainless-steel cladding on the Pressurized Water Reactor (PWR) in the nuclear plants and its impacts on warm water environments. A number of published articles of relevance to this study were selected. The most relevant papers were carefully selected, evaluated and reviewed. We included studies that were published in English and reported current issues on the behavior of 308L cladding material and their effects in the nuclear plant.

Important information was extracted from the selected relevant papers and characteristics were recorded according to the research of the articles. At the end of every topic a summary of it was given and recommendation for further research on the particular topic was given as well. Finally, a conclusion containing our view and recommendation was given to future researchers.

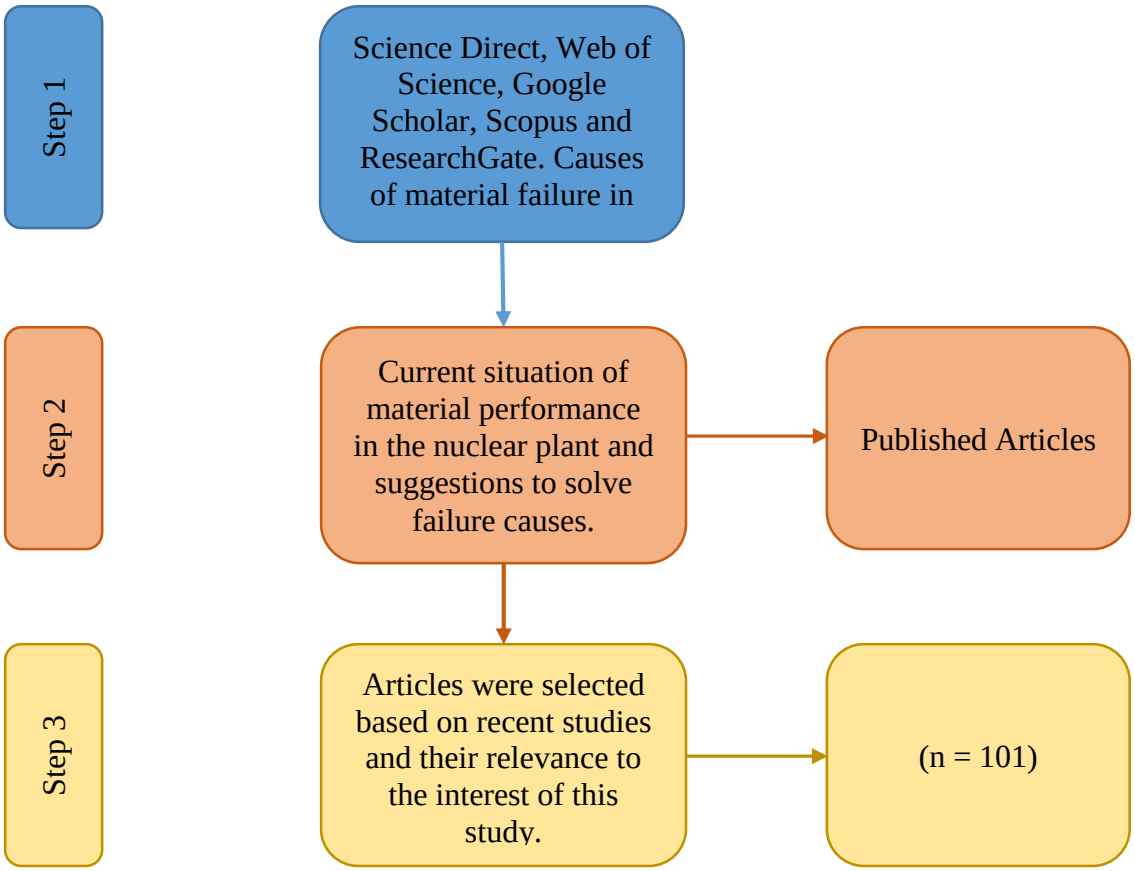

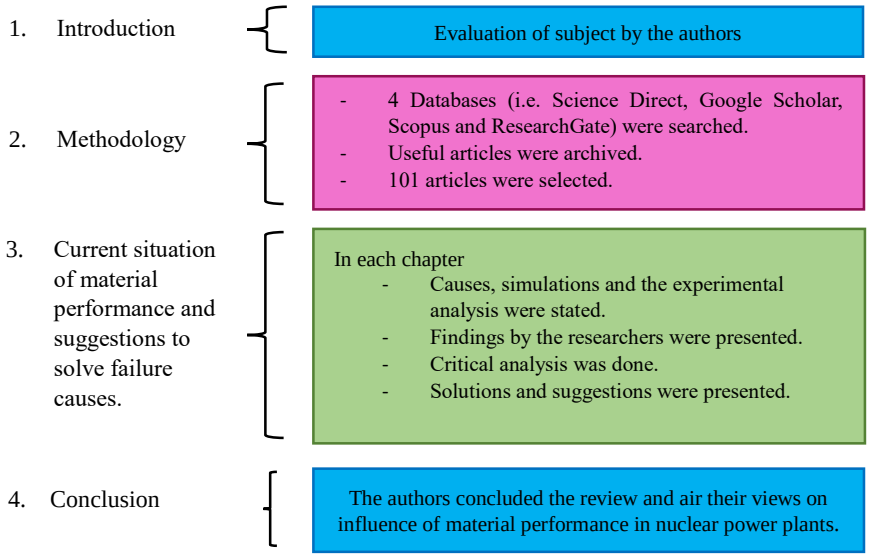

3. PARAMETERS OF STAINLESS-STEEL SURFACING WELDING

The nuclear power stainless-steel surfacing process is generally divided into two types; ESW and SAW. There are differences between the two types of welding processes. Regardless of the welding process mentioned, the stainless-steel surfacing layer after welding must meet the following conditions [1]:

(1) The stainless-steel clad layer is three-layer, one-layer transition layer and two-layer corrosion resistant layer. During the clad welding, the arc is stable, the splash is small, the slag can be removed easily, the welding seam is beautiful, the lap joint is good, the surface is smooth and has good crack resistance.

(2) The permeation detection method (PT method) shall check the surface defects of the surfacing layer and shall be free from defects such as pores, cracks, meat bites and slag inclusion.

(3) The internal defects of the surfacing layer shall be checked by the ultrasonic detection method (UT method) without excessive slag inclusion, crack, non-fusion and porosity, etc.

(4) The thickness of the clad layer should not be less than 6 mm, and its chemical composition should meet the corresponding standard requirements;

(5) The structure of the surfacing layer contains a certain amount of ferrite and the content of ferrite should be between 5% and 12%.

(6) There is no inter-crystalline corrosion tendency when the surface of the cladding layer is 2 mm down.

After qualified welding, relevant test items and assessment requirements are required to conduct a series of analysis on the performance of the stainless-steel clad layer. Thus, it can be seen that stainless-steel hard surfacing layer under the environment of nuclear power performance to a large extent affect the security and stability of the plant, because it strictly controls the surfacing layer in the actual performance of the service environment, the stainless-steel surfacing layer in real organization and performance changes of service environment, thus to provide a guarantee to the safe operation of nuclear power plant.

3.1 Composition and structure of stainless-steel hard surfacing layer

Table 1 shows the chemical composition of the materials used in the stainless-steel weld layer in the nuclear power plant [4]. As can be seen from the table, 309L stainless-steel has higher Chromium (Cr) and Nickel (Ni) content, in order to ensure that its composition is still similar to that of 308L stainless steel after being diluted by the parent material.

Table 1. Chemical composition of materials for stainless steel weld bead layer [9-11]

Materials	C	Si	Mn	Cr	Ni	S	P	Fe	Mo	Cu	Al	Nb
309L	0.011	0.3	1.8	23.35	13.36	0.001	0.011	Bal.	-	-	-	0.01
308L	0.011	0.34	1.69	19.74	9.96	0.010	0.016	Bal.	–	–	–	0.01

Ming et al. [6] calculated the Cr and Ni equivalent according to the chemical composition of stainless-steel surfacing layer of 309Land 308L stainless-steel, and based on the Schaeffler diagram stainless-steel surfacing layer were studied at room temperature. The experimental results showed that

stainless-steel surfacing layer (309L/308L) at room temperature are bipolar organization (austenite and ferrite), among them the content of ferrite is 5 ~ 10%.

The presence of a certain amount of ferrite can not only improve the strength of austenitic stainless-steel, but also reduce the thermal cracks of austenitic stainless-steel during welding [6-10]. But the presence of ferrite will produce adverse effect of austenitic stainless-steel, including decrease of austenitic stainless-steel and plastic and increases the tendency of austenitic stainless-steel forgings of thermal crack, to reduce the material performance of pitting and lead to organizational changes in high temperature environment such as sigma - eutectic carbides, which resulted in the failure of materials early [11 – 14].

Due to larger residual stress in welding, and for the whole of the three parts of stainless-steel surfacing outer shell, the existence of residual stress after welding is bigger and needs to be eliminated by Post-Weld Heat Treatment (PWHT) that is occurring in the process of relieving residual stress and the plant for stainless-steel welding layer, usually by heat treatment temperature of 600-650 ℃ [15-17].

Li et al [7] studied the different heat treatment post-weld temperature (650, 750 and 900 ℃) of 308L stainless-steel surface. Test results showed that with the increase of heat treatment of post-weld temperature in the 308L stainless-steel structure and the reticular continuous ferrite is interrupted to form the scattered bar ferrite. The study thinks that the reticular or flocculent ferrite is easy to cause the rapid crack expansion, while the bar ferrite can effectively avoid the rapid crack crossing, which leads to the increase of mechanical properties of the material.

Li et al [4-5] studied the influence of post-weld heat treatment on stress corrosion of stainless-steel surfacing welded joint. It was found that heat treatment increased the sensitivity of austenitic stainless-steel to stress corrosion (SCC), but not to a significant extent. The experimental results showed that the main influence of heat treatment is the element migration and microstructure change of welded joint, but the detailed results of microstructure analysis were not given.

Babu et al. [12] observed the changes of weld microstructure of 308L stainless steel after heat treatment through TEM, and found that the heat treatment would lead to a large amount of carbide on the interface between austenite and ferrite. Some researchers [13] found that the precipitation of carbides is related to the twin boundary and dislocation distribution in austenite.

Lo et al. [14] observed by transmission electron microscope that brittle station-phase occurs in the post-heat treatment surfacing layer, and the production of other precipitates is related to the composition of the material itself, while the corrosion performance of the stainless steel surfacing layer is largely dependent on the amount and distribution of the station-phase and M23C6 precipitation.

3.2 Oxidation behavior of stainless-steel surfacing layer

Slag, porosity and the existing defects will lead the stainless-steel to pitting corrosion pit initiation location due to welding processes. This makes the corrosion performance of stainless-steel point reduced. At the same time, the existence of heat treatment after welding can lead to material organization to form a new separation material after heat treatment, and the existence of new precipitates on the corrosion resistance of stainless-steel (inter-granular corrosion and pitting corrosion) with impact [14].For the stainless-steel surfacing layer, although the carbon content of the material itself has been

controlled below 0.03%, reducing the possibility of local corrosion caused by the massive release of carbide. However, due to the delay, disoperation or other uncertainties in the installation, debugging and operation of the pressure vessel, the ion composition and concentration in the water solution of the stainless-steel surface layer will deviate accordingly and lead to serious corrosion of the stainless steel hard surfacing layer [14].Also, due to nuclear power stainless-steel in high temperature and high-pressure water (operation temperature is 320 ℃, the pressure of 16 MPa) under the long-term corrosion, oxidation behavior of the stainless steel in high temperature water has also attracted a lot of attention and research.

3.2.1 Composition and structure with high warm water oxide film

Present literature [15] summarizes the research status of oxidation process and products of materials under high temperature and pressure water environment, including the composition and the structure of the oxide film formation mechanism and influencing factors, were discussed in this paper. The author thinks that material in high temperature and high-pressure water oxidation film of double-layer structure, are basically lining for Cr layer, outer layer for rich Fe oxides (stainless steel) or rich Ni oxide (Ni base alloy).

Many literatures have also studied and analyzed the structure and composition of surface oxidation film of stainless-steel and nickel-based alloy under high temperature and pressure water environment via a series of characterization methods such as TEM and XPS [16-24]. The inner layer of stainless-steel surface oxidation film is rich in Cr, and the outer layer is rich in Fe and Ni [25]. Moreover, as the growth rate of outer oxide particles is higher than that of the inner layer compact oxide film [26], the thickness of the outer oxide film is significantly higher than that of the inner layer.

Also, many researchers have observed that the oxide film on the outer layer of stainless-steel is mainly composed of loose and larger oxide particles, while the inner layer is small and compact oxide film. However, the composition, quantity and size of these surface oxide particles are related to the material composition [23, 24, 27], temperature [26, 28-30], dissolved oxygen content [19, 28, 29, 31], hydrogen (zinc) content [33, 32-34] and surface state [35-38].

Takumi et al. [23] reported the effect of different Cr contents on the surface oxidation film of stainless steel. The increase of the content of Cr can lead to outer oxide particle number and size of the change. Further analysis on the research results showed that the increase of the content of Cr generates denser alloy surface oxidation film, resulting in the formation of less outer oxide particles. Therefore, the high temperature water oxidation behavior of specific materials needs to be studied and observed.

Ming et al. [25] studied the influence of the change of surface state of 308L stainless-steel surfacing layer on the composition and structure of oxide film under high temperature and high-pressure water environment.

Caoet al.[27] studied the composition of 308L oxide film on the surface of stainless-steel surfacing layer through transmission electron microscopy and found that the composition of 308L oxide film is mainly sharp-like oxide $FeCr_2O_4$ and Cr_2O_3, which is consistent with other stainless-steel surface oxidation film components.

3.2.2 Mechanism of formation of water oxidation film at high temperature

Currently, for the molecular dynamics model of the formation of oxide film on the surface of materials, the most accepted theory is the Point Defect Model (PDM) proposed by Digby. D. Macdonald [40-41]. The model material surface oxidation film generated mainly exist in the process of three kinds of point defects (cationic vacancies V_m^{x+}, cationic clearance M_i^{x+} and anionic vacancy $V_o^{\cdot\cdot}$).On the one hand, some of the metal substrate dissolved cat ion and anion clearance space formation, as well as cat ion and anion clearance space to oxide film/solution interface movement and cationic clearance dissolved to form cat ions in the solution. In preparation for the next dehydration deposition (reaction (5)), anionic space formed by reaction and solution of the oxide film anion (reaction (6)), at the same time. Another part of the metal substrate directly formed the cat ion of oxide film (reaction (1) and (2)), the combination of cationic and anionic bits form oxide film on the surface of the material; Oxide and oxidation film. On the other hand, cat ion will occur, the corresponding solution in forming metal cat ion in solution and in diffusion of cationic vacancy and cationic vacancy as well as the reaction of the metal substrate can also generate further oxidation film of cat ion (reaction (1)), and it will result in an increase in material surface oxide. It is the diffusion of these three point defects at the metal matrix/solution interface and the interaction with the matrix and solution (reaction (3) and (7)) that leads to the formation and change of the surface oxidation film.

Many current literatures not only confirm the correctness of point defect model through room temperature electrochemical method or corrosion experiment, but also use point defect model to apply to more environmental studies. Fattah-Alhosseini et al. [43] used the point defect model to study the semiconductor properties of the passivating film on the surface of stainless steel, and obtained the concentration of point defect in the passivating film of 316 and 321 stainless-steel and the corresponding point defect diffusion factor values. Geringer [40] combined PDM, studied the mechanism of wear corrosion on the surface of materials and established the micro wear corrosion model on the surface of stainless-steel.

As the PDM model is mainly aimed at the growth model of oxide film at room temperature or low temperature, it has good and high-pressure water environment. The PDM model has certain limitations and imperfections. For example, it cannot fully explain the formation of loose oxide layer on the outer layer, the change of metal ion valence in high temperature water, diffusion dissolution deposition reaction etc. with detailed explanation. Therefore, some studies based on the point defect model were proposed on the basis of Mixed Conduction Model (MCM) [20, 21, 43-45].

The element considered in this model is Cr layer of the oxide film formed by solid growth, relative to the outer layer of the porous oxide film. The inner oxide film less dissolved and faster, so the K2 and K4 response compared with metal ions dissolved on the kinetics of the basic can be ignored, and the formation of outer oxide mainly depends on the metal Fe, Ni dissolving diffusion and deposition reaction (K1i, K3i and Kr).As a result of Fe and Ni elements in high temperature water dissolved quantity are very few, therefore diffusion deposition reaction has been in a local dynamic balance, leading to the formation of local large sized oxide particles. Meanwhile, in MCM model, the passivation dissolution of Cr element under high temperature and high pressure is also considered. Cr element is considered to be able to form Cr ions in a +6 valence state to be dissolved into the solution, which generally can only

occur under low potential and high temperature. This also explains the Cr element contained in the outer oxide film of stainless-steel in many literatures [43-46].

Based on the above molecular dynamic principle of oxide film formation, many literatures reported the formation mechanism of oxide film formation in the high-temperature water environment. The main formation mechanism can be divided into three types [22]; (1) both internal and external layers of oxide film are formed by solid growth;(2) the oxide film is formed by the dissolution and re-deposition of metal ions;(3) the inner layer of the oxide film is solid growth, while the outer layer of the oxide film is formed by the dissolution and re-deposition of metal ions. Although there is no unified conclusion on the formation mechanism of oxide film under high temperature and high pressure of stainless-steel at present, a large number of literatures have reported that the third mechanism is more consistent with the corrosion mechanism of stainless-steel under high temperature and high-pressure water. Xu et al. [46] studied electrochemical test methods such as confirmed by XPS, high temperature and the corrosion of 304 stainless-steel in high temperature water environment model. In this model, Cr element mainly through solid growth and rich Cr oxide film on stainless-steel surface, and the element of Fe. Ni first dissolve in the form of ion diffusion in the solution, then attached in the specimen surface in the form of natural gas hydrates. Part of the natural gas hydrates will pass dehydration condensation and generate the corresponding oxide particle deposition in the surface of the stainless-steel sample, thus forming the outer layer of the porous oxide film. The growth pattern of oxide film on stainless-steel surface has also been confirmed by many literatures [24-25, 27, 35].

For the metal ion dissolution and deposition phenomena in the growth process of stainless-steel oxide film, some literatures quantitatively characterize the ion solubility in the growth process of oxide film of material [47-49].Hamm et al. [47] measured the solubility of Fe and Cr elements in the formation process of alloy oxide film by ICP-AES, and the test results showed that Cr content in the alloy had a great influence on the solubility of metal ions in the process of material corrosion. Schmutz et al. [49] found that the mass dissolution of Fe in Fe-25Cr alloy led to the enrichment of Cr elements in the passivation film, and the dissolution of Fe ions was affected by potential and solution environment. The above results indicate that specific studies and quantitative characterization are needed for specific materials to characterize their ion dissolution and oxidation in service environments. Presently, the characterization of metal ion solubility and oxidation of stainless steel in high temperature and high-pressure water environment is not reported.

The thermal aging phenomenon refers to the phenomenon of the toughness and ductility of stainless-steel, especially dual-phase stainless-steel, decrease and the increase of time and the hardness and brittleness increasing during the long-term service process. After the thermal aging of stainless-steel, brittle fracture can easily occur in the material, leading to the occurrence of accidents [50].The stainless-steel thermal aging reason mainly lies in the dual phase austenite ferritic stainless steel. The organization are divided into the alpha phase and the rich, and the rich in Fe-Cr meeting of α'and αphase, makes the ferritic phase embrittlement and thus led to the serious decrease of the material fracture toughness [52].As for the stainless-steel hard surfacing, 5-12% ferrite exists in its structure, so the thermal aging behavior of the stainless-steel surfacing is also worthy of attention and research.

3.3.1 Stainless-steel tissue after thermal aging

According to a large number of literature reports [8-11 , 50-57], stainless-steel reduced thermal aging embrittlement mainly as a result of the following factors; (1) the ferrite internal modulation to produce the alpha phase and the rich phase of rich Fe-Cr α'phase;(2) G-phase precipitation in ferrite rich in Ni, Mn and Si;(3) carbide precipitation at the interface between austenite and ferrite. Tissue changes after thermal aging will be discussed below.

According to spinodal theory, due to the miscibility gap in the alloy system, two phases with the same crystal lattice type, different components and properties will be separated by slope diffusion rather than nucleation under certain thermodynamic conditions. This phase separation occurs in a narrow region between the inflection points of the free energy - composition curve. The amplitude modulation decomposition happens in the binary system, which can lead to system due to the composition fluctuation losing stability and appears increasingly in composition fluctuation amplitude and finally broken down into two phases. For ferritic stainless steel, the decomposition of amplitude modulation and two phases mainly forms after the alpha phase and the rich of the rich Fe-Cr α'phase[58].

Takeuchi et al. [9-10] used APT technology to observe the change of the amplitude modulated decomposition degree of Fe-Cr in ferrite of stainless-steel surfacing layer with thermal aging time. The results showed that the intensity of amplitude modulation decomposition of ferrite increases rapidly and slowly with the increase of thermal aging time.

Chandra et al. [50] found "spots" in ferrite after thermal aging through transmission electron microscopy, which has been proven by many literatures to be a feature of amplitude modulation decomposition in ferrite [53, 56, 60, 61], in which the intensity of amplitude modulation decomposition in ferrite can also be represented.

In addition to the amplitude modulation decomposition, G-phase will also precipitate in ferrite. According to literatures [55, 62-64], G-phase, chemical formula is Ni(Fe, Mo)16Mn(Ti, V, Nb, Cr)6Si7, face centered cubic structure, and its lattice constant is 1.09-1.14nm.The experimental study found that the composition of G-phase is related to the chemical composition of the material itself, and table 2 is the composition of G-phase in various stainless-steel materials. It can be seen from the table that specific analysis of G-phase composition is required for specific materials.

Table 2. composition of G-phase in different stainless-steel materials [63]

Material	**Aging Condition**	**Method**	**Compositions of G-phase (wt%)**					
			Fe	**Cr**	**Ni**	**Mn**	**Si**	**Mo**
Z3CN20-09M	400℃, 20,000h	EDS	59.12	27.55	3.85	3.57	5.91	-
SCS14A	400℃, 10,000h	EDS	53.7	20.2	13.3	0	4.9	5.9
AISI 329	475℃, 4000h	EDS	42.18	29.24	12.43	4.39	5.31	6.45
CF8M	450℃, 10,000h	EDS	15.8	25.4	26.4	2.7	14	15.7
CF3M	350℃, 200,000h	APT	39.7	15.6	22.6	4.5	11.4	6.2

Li et al. [53, 56]found that for Z_3CN_{20}-9m stainless-steel 400℃ heat aging tissue was studied, and the experimental results showed that the G-phase in thermal aging time has reached around 10000h to precipitate, and precipitation of G-phase the size is small, the average size of nano level. Chen et al.

[63] showed that the size and distribution of G-phase were related to the carbides at the phase interface. The G-phase distribution near the carbides was sparse but the average size was large. Some literatures believe that the existence of amplitude modulated decomposition is the root cause of the formation of G-phase in ferrite, and since the generation of amplitude modulated decomposition requires a long time of gestation, G-phase can be formed after a long time of thermal aging.

According to literature [86], the precipitation of carbides along the phase interface is also one of the reasons leading to the brittle failure of materials. Therefore, it is worthy of attention.

3.3.2 Mechanical properties after thermal aging

Chandra et al. [50] measured the ferritic hardness of 304L and 316L stainless-steel after thermal aging through nano hardness, and the test results showed that the ferritic hardness of stainless-steel increased monotonously with the increase of thermal aging time. And Li [53, 56]found that the Z_3CN_{20}-09 m ferrite stainless-steel hardness increased with thermal aging time is nonlinear. Ferrite phase modulation break down to form the α and α'phase embrittlement because α and α' phase of the lattice constant is different. So, in the interior of the ferrite phase will form a large number of coherent strain field, resulting in dislocation glide impeded, making ferritic phase cirrhosis [53, 56].The ferrite phase after hardening must undergo plastic deformation in a twin-like manner [60], so the cleavage crack can be in the inner core of the deformation twins, resulting in cleavage fracture, which results in the decline of mechanical properties of materials.

Li et al. [52] found through the mechanical property test that thermal aging has a great impact on the mechanical property of stainless-steel, especially on the impact property. The longer thermal aging time is, the worse the material impact property is. A large number of literatures [53, 54, 56, 66-69] on stainless-steel after thermal aging studied the microstructure and mechanical properties. The results showed that ferrite phase precipitation after aging for a long time the dispersion of $\alpha'$and a small amount of G-phase, and that α' phase is composed of ferrite phase decomposition generated amplitude modulation, casting austenitic stainless steel is the main cause of thermal aging embrittlement, G-phase as opposed to the influence of material mechanics performance is not obvious.

The mechanical test results of Chandra et al. [50] also confirmed the impact of thermal aging on the impact performance of stainless-steel. Chandra et al. believed that the co-existence of amplitude modulated decomposition and G-phase led to changes in the mechanical properties of materials. Chung et al. [69] carried out aging experiments on CF-3, CF-8 and CF-8m grades stainless steel with different composition and ferrite content. By measuring the Charpy impact energy of CF-3, CF-8 and CF-8m grades stainless steel samples with different temperature and aging time, the kinetics of thermal aging embrittlement was obtained, and the activation energy model was proposed. According to the activation energy model, Ni-Si, Mo-Si, Ni-Mo-Si polymerization and subsequent G-phase precipitation and ferrite-austenite phase boundary $M_{23}C_6$ precipitation would hinder the decomposition of ferritic phase spinodal, reducing the activation energy of the material. Moreover, the hindering effect of the former was larger, thus reducing more.

The fact that traditional tensile and impact tests to a great extent waste a lot of material, there is need for a more convenient and safe material test method to the related performance. Analysis was

carried out on the equipment in service; the small punch test method is a kind of approximate half non-destructive detection method. Its detection has characteristics of fast speed and accuracy, with the sample size requirement being very small (generally for ϕ 10 mm, thickness of 0.5 ~ 1 mm) [85-89].Therefore, very suitable for some on-line inspection of the equipment in service. It is also widely used in the analysis of mechanical properties of thermal aging materials. Cheon et al. [70] analyzed mechanical embrittlement behavior after thermal aging through the method of small punching hole test and the test results showed that the energy of small punching hole gradually decreased with the increase of thermal aging time and the brittleness of materials gradually increased. Jang et al. [81] tested the mechanical properties of the samples after thermal aging and re-recovery by stretching and small punching tests, and successfully characterized the changes in the properties of the samples after thermal aging and re-recovery, indicating that the small punching test is very suitable for the mechanical properties characterization of the samples before and after thermal aging.

However, due to the existence of amplitude modulation decomposition, G-phase and carbide in the microstructure of the stainless-steel surface layer after thermal aging, the influence of these three factors on the mechanical properties of the stainless-steel surfacing layer has not been clearly defined. At the same time, in order to realize the thermal aging test of stainless-steel surfacing layer, it is necessary to observe and analyze the mechanical properties change of small punching holes before and after the thermal aging of stainless-steel surface layer. However, there is presently, still no research on the small punching test of stainless-steel surfacing layer. Therefore, it is necessary to study and analyze the mechanical properties of stainless-steel surfacing layer before and after thermal aging.

3.3.3 Deformation behavior after thermal aging

Due to the presence of ferrite and austenite phases in stainless-steel tissues, the composition differences of the two phases will lead to different responses to deformation, so the deformation behaviors of the two phases are also different [83-88].In the literature [82], it is believed that there are two deformation mechanisms of ferritic phase in duplex stainless steel as; (1) the dislocation in austenite phase is concentrated at the phase interface, and the stress concentration at the interface drives the dislocation slip within the ferritic phase, thus the corresponding slip line appears in the ferritic phase; (2) ferrite phase is directly subject to the shear action of adjacent austenite phase, and the slip line formed in austenite phase directly passes through the ferrite phase, thus forming a coherent crossing slip line. Dr. Serre [82] studied the dual phase steel observation of the deformation behavior of the system and summary. The study thought the first deformation occurred in the organization is relatively soft, austenitic phase can form dense linear slip band, and the organization of the ferrite deformation method on the one hand, influenced by its own deformation. On the other hand, also comes from the surrounding deformation austenite phase, in the process of deformation, the austenite phase forming first slip band will be extended to the ferrite, and plastic of ferrite and austenite phase around coordination finally determines the type of phase slip band. He systematically summarized four slip bands in the ferrite phase, which are; (1) continuous linear slip bands, or A2 type slip bands for short. There is good deformation coordination between the austenite phase and ferrite phase. The deformation in the austenite phase can smoothly drive the ferrite phase to undergo the deformation process. Therefore, the linear slip belt

throughout the ferrite phase can be produced;(2) short linear slip belt, namely A1 slip belt. The deformation of austenite phase can only drive the ferrite phase at the phase interface to deform, but there is no obvious deformation behavior in the ferrite phase, so only a certain length of slip band can be generated at the phase interface; (3) semi-curved slip belt, referred to as F2 slip belt. The slip band is formed on the basis of A1 slip band, and the corresponding deformation behavior is generated in the ferrite phase independently;(4) completely curved slip belt, referred to as F1 slip belt. The deformation coordination between austenite phase and ferritic phase is poor, and ferritic phase can only pass through autonomous deformation. Therefore, a completely curved slip belt is produced inside the ferritic phase.

For stainless-steel after heat aging, because of the ferrite phase modulation of decomposition and G-phase, to harden ferrite in the deformation process is very difficult to produce corresponding deformation and slip band, reducing the deformation coordination of austenite and ferrite phase. Thus, bring about sclerosis of austenite and ferrite phase interface stress concentration, eventually lead to the increased brittleness of materials and mechanical properties. So, thermal aging behavior after deformation in each phase of the research is particularly important.

Li et al. [53, 54,55, 85] through the tensile experiment, found that after thermal aging of ferritic phase appear a lot of deformation twin, and the emergence of these mechanical twin for micro crack initiation provide certain conditions. They believed the process of drawing, decomposition and the existence of the G-phase will lead to a large number of forming inside the ferritic phase coherent strain field, leading to large numbers of dislocations linked together. The slip has been hampered, eventually leading to the generation of mechanical twin. Wang et al. [87] used homemade tensile fixtures on centrifugal casting of stainless-steel after heat aging deformation observation. They found that the thermal aging in front of the ferrite phase appeared in the process of stretching A1, A2, F1 and F2 type of slip band. However, after thermal aging of the ferrite phase only a cross slip band, the appearance of slip band can also lead to micro crack initiation. They also found that the slag and carbide existence of the second phase will lead to the crack initiation and rapid failure.

To sum up, after thermal aging deformation of austenite and ferrite phase mode has no unified conclusion and no systematic research. Therefore, tissue deformation after thermal aging behavior also requires further in-depth study and summary. Also, it does not take into account the exudates and the existence of quadratic phase of thermal aging material model of deformation and fracture behavior of influence which also needs further research and analysis.

3.3.4 Corrosion behavior after thermal aging

The stainless-steel after heat aging tissues and many separation material existence not only leading to the change of material mechanical properties, as well as the influence on the corrosion performance of changes, but including point between corrosion and corrosion resistance have been widely studied [91].The results showed that the existence of amplitude modulation decomposition of poor Cr the ferrite, which increases the thermal aging material local corrosion sensitivity [92-99].

Wang et al. [90] measured the pitting corrosion of stainless-steel after heat aging properties. The experimental results showed that with the increase of thermal aging time, materials, pitting the pit initiation location from austenitic stainless-steel, to the organization gradually into initiation with ferrite

to austenite.The study confirmed in the ferritic am decomposition and the existence of the G-phase will reduce material corrosion performance.

Ren et al. [89] studied the thermal aging for nuclear power main Z_3CN_{20}-9 m stainless-steel pitting, affecting the performance of their Z_3CN_{20}-9 m stainless-steel tube at 400℃ of 0-10000h thermal aging experiments, and the part of the aging test was 550℃ heat 1h annealing treatment and then by the method of polarization and electrochemical impedance (EIS) measured the pitting corrosion properties of the materials. The results showed that the material of pitting corrosion potential and corrosion resistance decrease with the extension of thermal aging time. Thermal aging materials after 550℃ annealing treatment after 1h of pitting corrosion potential and corrosion resistance are restored to the level of material aging.

For Zhang et al. [89], electrochemical potentio-dynamic polarization and constant electric potential, critical pitting temperature method, studied the aging at 700℃ UNSS82441 duplex stainless-steel in different time of pitting corrosion performance. The results showed the extension of aging time and the pitting corrosion properties of the materials.

Yi and Shoji [90], Park and Yoon[91] found that the corrosion current density and dissolution rate of ferritic phase in the austenitic stainless-steel cast by thermal aging in an acidic environment increased with the extension of thermal aging time, and the corrosion resistance of the material decreased.

Rovere et al. [92] used electrochemical methods to test inter-crystalline corrosion performance of dual-phase stainless steel after thermal aging. The test results showed that a large number of lean Cr areas were generated inside ferrite after thermal aging, which seriously reduced the anti-inter-crystalline corrosion ability of the material.

Kim et al. [98] studied by Raman spectroscopy A152 - LAS dissimilar welding of welded joint of high temperature water corrosion behavior. The test results showed that heat aging can lead to the change of the welding joint surface oxide, the reason is due to thermal aging can lead to welding joint on both sides of the elements to move between, leading to a welded joint under the water environment of high temperature oxidation film composition changes.

Adem [100] investigated the effects of artificial aging heat treatment on mechanical properties and corrosion behavior of AA6XXX alloy. The results showed that increase in aging time increases the mechanical properties of the material and artificial aging time determines the corrosion resistance of the alloy. The best corrosion resistance value was obtained at a temperature of 190℃ at 10-h aging period.

Federica [101] investigated the effects of thermal aging on localized corrosion behavior of lean duplex steel (LDSS 2404) between temperatures 650 and 850℃. They studied intergranular corrosion (IGC) attack after double loop electrochemical potentiokinetic reactivation (DL-EPR) using optical method (OM) and scanning electron microscopy (SEM) and focused ion beam (FIB) integrated to SEM. The study observed that aging at 650℃ or 5minutes aging time at 750℃ caused nitride precipitation mainly at α/α grain boundaries due to fast diffusion of chromium in this phase. At 850℃ or 10-60 minutes at 750℃, aging allowed precipitation at α/ϒ interface. Based on electrochemical tests, they concluded that pitting attack only affected the α phase while in aged samples, pitting and IGC attack were detected near the nitrides in correspondence of α/α and α/ϒ grain boundaries depending on aging temperatures and times.

3.3.5 Summary of thermal aging behavior of stainless steel

For stainless-steel welding layer, because of its organization in a certain amount of ferrite (5 ~ 12%), low temperature hydrothermal aging for a long time can cause ferrite stainless-steel surfacing layer organization internal am decomposition, G-phase and carbides. So, the thermal aging behavior is also the focus of the study of stainless-steel clad layer. There are literatures only for stainless-steel surfacing layer of organization and mechanical properties, impact toughness and tensile properties [8-10, 65, 66]. However, there is no relevant report on the change of small punching test performance of the surfacing layer before and after thermal aging, and relevant data accumulation and analysis are not available. The analysis of the microstructure and properties of the stainless-steel surfacing layer after thermal aging has not been completed. Therefore, research on thermal aging behavior of stainless-steel surfacing layer still has the following problems:

(1) There is no systematic study and summary of the size, distribution rules and formation reasons of the precipitates in the stainless-steel hard surfacing tissue after thermal aging;

(2) Due to the existence of amplitude modulation decomposition, G-phase and carbides in the microstructure of the stainless-steel surfacing layer after thermal aging, the effects of these three factors on the mechanical properties of the stainless-steel surface layer have not been made clear.

(3) The deformation modes of the two phases of austenite and ferrite before and after thermal aging have not been systematically studied and unified conclusions have not been reached, and the role of precipitates in them has not been clearly observed and analyzed.

(4) After thermal aging, the existence of precipitates in the stainless-steel clad layer tissue has not been studied and reported, especially for the change of the material oxidation behavior and for the high-temperature water oxidation behavior.

4. CONCLUSION

There have been many reports on the research of nuclear power stainless-steel surfacing welding layer but there is a lack of techniques. The obtained data are relatively scattered, and the corresponding connection cannot be established between the experimental data. At the same time, based on the research of the stainless-steel surfacing layer literatures found, most of the studies have been focused on the performance of the organization and individual research and observations. However, based on the review, no study was found to have established the relationship between performance of the stainless-steel surfacing layer under high temperature and the high-pressure water environmental oxidation behavior from the perspective of oxidation corrosion mechanism of high temperature corrosion model. Also, the literatures did not consider organization and heat treatment after welding and the length of low temperature heat aging, on high-temperature water oxidation behavior of materials. Due to the late start of research on thermal aging behavior of nuclear power materials in many countries, there is inadequacy of complete and systematic research on the thermal aging of nuclear power stainless-steel hard surfacing layer. Similarly, no relevant studies and reports on the changes in the structure and performance of the stainless-steel surfacing layer before and after thermal aging was found. A detailed and systematic study

on the thermal aging behavior and corresponding corrosion performance of the key welding materials for the nuclear plant main equipment should be conducted. Firstly, the microstructure of stainless-steel surfacing layer before aging and its effect on corrosion performance should be studied. Then the evolution of the stainless-steel surface layer organization after thermal aging be observed and summarized. Finally, the mechanical damage and its behavior, influence of the oxide to establish clad welding of stainless-steel under the condition of long-term service and performance of evolution model should be studied to improve durability of main equipment of nuclear plant and provide certain theoretical basis and data support.

References

1. A. Robinson , and S. Bonell,*World Pumps*, 9 (2010) 4244.
2. A. Brown,,*World Pumps*, 469 (2005) 50.
3. I. Hamada, and K. Yamauchi, *Metall. Mater. Trans. A*, 33 (2002) 1743.
4. G.F Li, E.A. Charles , and J. Congleton, *Corrosion Science.,* 43 (2002) 1963.
5. G.F Li, and J. Congleton,, *Corrosion Science*, 42 (2002) 1005.
6. H.L Ming,Z.M. Zhang, and J.Q. Wang, *Mater. Charact.*., 97 (2014) 101.
7. K.B. Li, D. Li. and D. Liu,, *Appl. Surf. Sci*340 (2015) 143.
8. T. Takeuchi, Y. Kakubo, and Y. Matsukawa, *J. Nucl. Mater.*, 452 (2014) 235.
9. T. Takeuchi, J. Kameda and Y. Nagai, *J. Nucl. Mater.*, 425 (2012): 60.
10. T. Takeuchi,J. Kameda. And Y. Nagai, *J. Nucl. Mater.*, 415 (2011) 198.
11. N.V Rao, D.S. Sarma and S. Nagarjuna, *Mater. Sci. Technol.*, 25 (2009) 1387.
12. S.S Babu, S.A. David and J. M.Vitek, *Appl. Surf. Sci.*, 87 (1994) 207.
13. B. Sasmal, *J. Metall. Metall. Mater. Trans. A*30 (1999) 2791.
14. I. Lo and W.T Tsai, *Mater. Sci. Eng., A*, 255 (2003) 137.
15. I. Hamada and K. Yamauchi, *Nucl. Eng. Des.*, 214 (2002) 205.
16. E. Kikuti, N. Bocchi and J.L. Pastol, *Corrosion Science*, 49 (2007) 2303.
17. Q. Xiong, H. J. Li and Z.P. Lu, *J. Nucl. Mater.,* 498 (2017) 227.
18. W.J. Kuang, X.Q. Wu and E.H. Han, *Corrosion Science*, 52 (2010) 4081.
19. W. J. Kuang, X.Q. Wu, and E.H. Han E, *Corrosion Science*, 63 (2012) 259.
20. M. Bojinov, A. Galtayries and P. Kinnunen, *Electrochim. Acta*, 52 (2007) 7475.
21. M. Bojinov, P. Kinnunen P, and K. Lundgren, *J. Electrochem. Soc.*, 152 (2005) B250.
22. X.Q Cheng, Z.C. Feng and C.T. Li, *Electrochim. Acta*, 56 (2011) 5860.
23. T. Takumi, Y Takuyo and M. Tomoki, *J. Nucl. Sci. Technol.*, 45 (2008) 975.
24. G.D Han, Z.P. Lu and X.K. Ru, *Corrosion Science*, 106 (2016) 157.
25. H.L. Ming, Z.M. Zhang and J.Q Wang, *Appl. Surf. Sci.*, 337 (2015) 81.
26. H. Sun, X.Q. Wu and E.H. Han, *Corrosion Science*, 51 (2009) 2840.
27. X.Y Cao, X.F. Ding and Y.H. Lu., *J. Nucl. Mater.*, 467 (2015) 32.
28. F. Arjmand, L.F. Zhang, and J.M. Wang, *Nucl. Eng. Des.*, 322 (2017) 215.
29. L.J. Dong, Q.J. Peng and Z.M. Zhang, *Nucl. Eng. Des.*, 295 (2015) 403.
30. K. Wang, J.H. Wang, and W.B. Hu, *Mater. Des*, 82 (2015) 155.
31. H. Sun, X.Q. Wu and E.H. Han, *Corrosion Science*, 59 (2012) 334.
32. X.H. Liu, X.Q. Wu and E.H. Han, *Corrosion Science*, 53 (2011) 3337.
33. X.H. Liu, X.Q. Wu and E.H. Han, *Corrosion Science*, 65 (2012) 136.
34. S.H. Zhang, X.R. Shi and Y.Q. Chen, *J. Alloys Compd.*, 731 (2017) 1230.
35. Y. Takeda, T. Shoji, and M. Bojinov, *Appl. Surf. Sci*., 252 (2006) 8580.
36. J.L. Lv, H.Y. Luo and T.X. Liang, *J. Nucl. Mater.*, 466 (2015) 154.
37. J.L. Lv, T.X. Liang and H.Y Luo H, *Nucl. Eng. Des.*, 309 (2016) 1.

38. H.Y. Luo, Y.B. Zhang and H.B. Li, *J. Alloys Compd.*, 696 (2017) 1235.
39. D. Macdonald, *Electrochim. Acta*, 56 (2011) 1761.
40. D. Hamm, K. Ogle and C.O.A Olsson, *Electrochim. Acta*, 79 (2012) 17.
41. S. Lapuerta, N. Moncoffre and H. Jaffrezic, *Appl. Phys Express.*, 101 (2007) 277.
42. A. Fattah-Alhosseini, F. Soltani and F. Shirsalimi, *Corrosion Science*, 53 (2011) 3186.
43. I. Betova, M. Bojinov and P. Kinnunen, *J. Electrochem. Soc.*, 155 (2008) c81.
44. B. Beverskog, M. Bojinov and P. Kinnunen, *Corrosion Science*, 44 (2002) 1923.
45. B. Beverskog, M. Bojinov, and A. Englund, *Corrosion Science*, 44 (2002) 1901.
46. J. Xu, X.Q. Wu and E.H. Han, *Electrochim. Acta*, 71 (2012) 219.
47. D. Hamm, C.O.A Olsson and D. Landolt, *Corrosion Science*, 44 (2002) 1009.
48. D. Hamm, K. Ogle and C.O.A Olsson., *Corrosion Science*, 44 (2002) 1443.
49. P. Schmutz and D. Landolt, *Electsrochim. Acta*, 45 (1999) 899.
50. K. Chandra, V. Kain and V. Bhutani, *Mater. Sci. Eng., A*, 534 (2012) 163.
51. V.H.C.D Albuquerque, E.D.M. Silva and J.P. Leite, J. *Materials & Design*, 31 (2010) 2147.
52. S.L. Li, Y.L. Wang and S.X. Li, J. *Materials & Design*, 50 (2013) 886.
53. S.L Li, Y.L Wang and X.T. Wang, *Mater. Sci. Eng., A*, 625 (2015) 186.
54. S.L. Li, Y.L. Wang and X.T. Wang, *J. Nucl. Mater.*, 452 (2014) 382.
55. S.L Li, Y.L. Wang and H.L. Zhang, *J. Nucl. Mater.*, 433 (2013) 41.
56. S.L Li, H.L. Zhang and Y.L. Wang, *Mater. Sci. Eng., A*, 564 (2013) 85.
57. O. Soriano-Vargas, E.O. Avila-Davila and V.M. Lopez-Hirata., *Mater. Sci. Eng., A*, 527 (2010) 2910.
58. J. Wang, H. Zou and C. Li, *Mater. Charact.*. 59 (2008) 587.
59. Y.S. Li, S.X Li and T.Y. Zhang, *J. Nucl. Mater.*, 395 (2009) 120.
60. S.K. Shi, J. Yan and Y. Zhang, *Nucl. Eng. Des.*, 250 (2012) 167.
61. K.B. Alexander, M.K. Miller and D.J. Alexander, *Mater. Sci. Technol.*6 (2013) 314.
62. W.Y. Chen, M. Li and X. Zhang, *J. Nucl. Mater.*, 464 (2015) 185.
63. J.M. Vitek, *Metall. Mater. Trans. A*, 18 (1987) 154.
64. S.S. Babu, S.A David and J.M. Vitek,, *Metall. Mater. Trans. A*, 27 (1996) 763.
65. S.S. Shi, G.D. Ma and B. Guo, *J. Mater. Eng. Perform.*, 23 (2014) 2043.
66. J. Wang, H. Zou and C. Li, *Mater. Charact*, 57 (2006) 274.
67. Z.X. Wang, F. Xue and W.H. Guo, *Nucl. Eng. Des.*, 240 (2010) 2538.
68. Z.X. Wang, F. Xue and J.W. Jiang, *Engineering Failure Analysis*, 18 (2011) 403.
69. H.M. H. M. Chung and T.R. Leax, *Mater. Sci. Technol.*, 6 (1989) 249.
70. J.S. Cheon and I.S. Kim, *J. Nucl. Mater.*, 278 (2000) 96.
71. J.M. Alegre, I.I. Cuesta and P.M. Bravo, *Procedia Eng*, 10 (2011) 1007.
72. E. Altstadt, H.E. Ge and V. Kuksenko, *J. Nucl. Mater.*, 472 (2016) 186.
73. M.A. Contreras, C. Rodríguez and F.J. Belzunce, *Fatigue Fract. Eng. Mater. Struct*, 31 (2008) 727.
74. J. Kłaput, *Arch. Metall. Mater*, 60 (2015) 47.
75. I.I. Cuesta, J.M. Alegre and V. Ortega-López, *Mater. Des*, 83 (2015) 363.
76. T.E. García, C. Rodríguez and F.J. Belzunce, *J. Alloys Compd.*, 582 (2014) 708.
77. S.H. Hong,M.G. Seo and C.H. Jang, *Procedia Eng.*, 130 (2015) 1010.
78. M. Song, K.S. Guan and W. Qin, *IOP Conf. Ser.: Mater. Sci. Eng*, 606 (2014) 346.
79. M. Song, N.P. Gurao and W. Qin, *IOP Conf. Ser.: Mater. Sci. Eng*, 628 (2015) 116.
80. H. Jang, S. Hong and C. Jang, *Materials & Design*, 56 (2014) 517.
81. C. Jang, H. Jang and S. Hong, *International Journal of Pressure Vessels and Piping*, 131 (2015) 67.
82. I. Serre, D. Salazar and J.B. Vogt, *IOP Conf. Ser.: Mater. Sci. Eng*, 492 (2008) 428.
83. S. Fréchard, F. Martin and C. Clément., *IOP Conf. Ser.: Mater. Sci. Eng*, 418 (2006) 312.
84. Y. Wang, Y.H. Yao and Z.P. Wang, *IOP Conf. Ser.: Mater. Sci. Eng*, 666 (2016) 184.

85. S.L Li, Y.L Wang, and X.T. Wang, *IOP Conf. Ser.: Mater. Sci. Eng*, 639 (2015) 640.
86. G. Liu,Y.L Wang and S.L. Li, *Mater. High Temp*, 33 (2016) 1878.
87. S.L. Li, Y.L. Wang and X.T. Wang, *Mater. High Temp*, 32 (2015) 524.
88. Y.Q. Wang, B. Yang and J. Han, *Procedia Eng*, 36 (2012) 88.
89. Z.Y. Zhang Z Y, Zhao and H.Z. Zhang, Corrosion Science, 93 (2015) 120.
90. Y.S. Yi and T. Shoji, *J. Nucl. Mater.*, 231 (1996) 20.
91. J.S. Park and Y.K. Yoon, *Scr. Metall. Mater*, 32 (1995) 1163.
92. C.AD. Rovere, F.S. Santos and R. Silva, Corrosion Science, 68 (2013) 84.
93. R. Silva, L.F.S. Baroni and C.L. Kugelmeier, J. Corrosion Science, 116 (2017) 66.
94. R. Silva, L.F.S. Baroni and M.B.R Silva, *Mater. Charact.*, 114 (2016) 211.
95. R. Silva, C.A Della Rovere and S.E. Kuri, *Mater. Sci. Forum*, 869 (2016) 705.
96. Y.F. Chen, B. Chen and F. Dong, *Eng. Fail. Anal*, 83 (2018) 1.
97. K. Chandra, V. Kain and V.S. Raja, Corrosion Science54 (2012) 278.
98. J. Kim, k.J. Choi and B.B. Chi, *J. Nucl. Mater.*, 449 (2014) 181.
99. J.M. Vitek and S.A. David, J. Eng. Fail. Anal, 2018,83;1-8
100. O. Adem, *J. Chem. Eng. and Mater. Sci.*, 9 (2018) 17.
101. Z. Federica, G. Vincenzo, B. Andrea, Z. Fabrizio and M. Cecilia M, Metals, 9 (2019) 529.